JOURNAL OF CHEMICAL INFORMATION AND MODELING

Article

pubs.acs.org/jcim

Docking Simulation Study and Kinase Selectivity of f152A1 and Its Analogs

Megumi Ikemori-Kawada,[†] Atsushi Inoue,[†] Masaki Goto,[†] Yuan John Wang,[‡] and Yoshiyuki Kawakami[†,*]

[†]Eisai Tsukuba Research Laboratories, 1-3, Tokodai 5-chome, Tsukuba-shi, Ibaraki 300-2635, Japan

[‡]H3 Biomedicine Inc.,300 Technology Square, Cambridge, Massachusetts 02139, United States

ABSTRACT: f152A1 is a potent inhibitor of MAP kinases and TNFα-transcription. When f152A1 and its analogs are assayed against ERK2, MEK1, and MEKK1, these compounds show different inhibition profiles. It is considered that the highly reactive *cis*-enone moiety and modifications of the 14-membered resorcylic lactone ring may determine their kinase selectivity and potency. In order to clarify the different potencies of these compounds toward MAP kinases, conformational analysis, molecular orbital studies, and docking simulation studies using model structures of ERK2, MEK1, and MEKK1 have been performed. These studies have revealed that (i) ligand binding does not depend on chemical bonding but on molecular interaction (molecular orbital analysis), (ii) the *cis*-enone moiety of inhibitors is in the range of Michael addition reaction with the Cys166 residue in ERK2 (docking simulation study), and (iii) molecular shape of M1(8) conformations is the best fit for the ATP binding site of kinases. Considering the molecular docking analysis of these inhibitors in these kinases, molecular shape will be most important to their corresponding kinases activities.

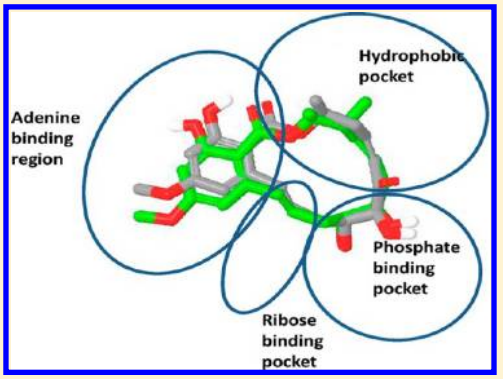

INTRODUCTION

During the course of screening for the inhibitors of TNFα transcription, f152A1 (**1**), (3*S*,5*Z*,8*S*,9*S*,11*E*)-8,9,16-trihydroxy-14-methoxy-3-methyl-3,4,9,10-tetrahydro-1*H*-2-benzoxacyclotetradecine-1,7(8*H*)-dione, isolated from the fermentation broth of a fungus, *Curvularia Verruculosa,* was identified (Figure 1).[1] f152A1 and its analogs were later found to be potent inhibitors of signaling molecules and pathways distal from MEKK1 such as MEK1 and ERK1/2. These kinase inhibitory activities were believed to contribute to their inhibition of immune response and cell proliferation. f152A1 is readily metabolized in biological fluid, because of a highly reactive *cis*-enone moiety in the 14-membered resorcylic ring. The medicinal chemistry effort aiming to improve stability and obtain s desirable in vivo pharmacological effect resulted in synthesis of over 400 analogs. E6201 emerged as a promising candidate with favorable metabolic stability, desirable kinase profile, and potent in vivo efficacy.[2−5]

We previously reported results of conformational analysis and molecular orbital studies of f152A1 and its analogs in line with structure−activity relationship (SAR) data on the *cis*-enone moiety and 14-membered resorcylic acid lactone ring, where we found that (i) the enone is likely a Michael acceptor; (ii) the active conformation is M1(8), in which an intermolecular hydrogen bond between 8-OH and the enone oxygen increases reactivity of the enone moiety; and (iii) the 8,9-diol restrains the 14-membered ring conformation.[6]

The X-ray crystal structure of the ERK2 in complex with FR148083(f152A1)[7] suggested that the compound binds to the ATP binding site of ERK2 and forms a covalent bond with Sγ of ERK2 Cys166. This indicated that both the *cis*-enone and the conformation of the 14-membered resorcylic lactone ring contribute to this inhibitory activity. The authors concluded that covalent bond to the common cysteine residue in the ATP-binding site is likely to play a crucial role in the inhibitory activity against MAP kinases. Consistent with these findings, it has also been reported that hypothemycin inhibits a subset of ∼45 known Ser/Thr/Tyr protein kinases containing a cysteine residue corresponding to Cys166 of ERK2.[8] The recent molecular modeling studies and the crystal structure of an ERK2−hypothemycin complex suggest that hypothemycin[9,10] also forms a similar complex as f152A1 in which the Sγ of the cysteine approaches hypothemycin from the reface of the double bond and forms a covalent adduct with R-stereochemistry.[11]

In the C4 modified analogs of f152A1, it was particularly noted that C4 methyl showed considerable improvement in metabolic stability, while having modest potency. Compound **2** (ER-803064) retained the cell report or potency (IC_{50} = 136 nM) and improved mouse plasma stability (>80% remaining vs 2.5% of f152A1 in 2 h incubation).[3] Although the in vitro potency of compound **2** in suppressing LPS-stimulated cytokines productions from macrophages decreased by nearly 10-fold, the short-term LPS challenge the in vivo model showed stronger suppression of cytokine production (IL-6) in mice than f152A1 (**1**) at similar dosing. As reported by Goto et al.,[12] ER-803064 (**2**), the C4 methyl analog of f152A1, lost inhibitory

Received: March 13, 2012
Published: July 25, 2012

dx.doi.org/10.1021/ci300135g | *J. Chem. Inf. Model.* 2012, 52, 2059−2068

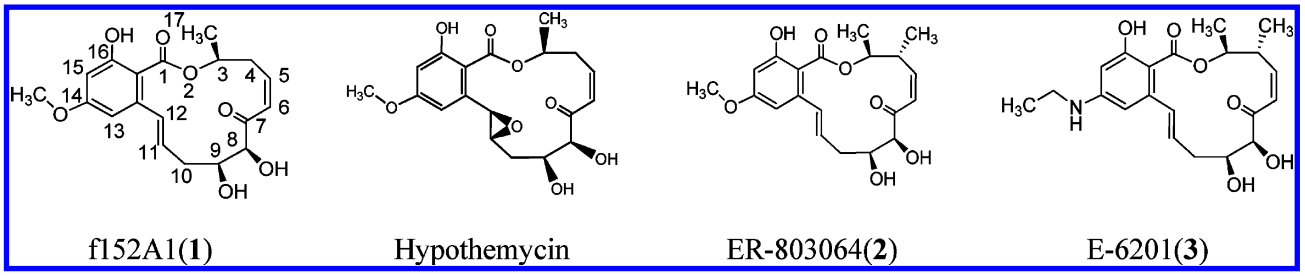

Figure 1. Molecular structures of f152A1 and its analogs.

Table 1. Effects of f152A1, ER-803064, and E6201 on MAPK Family's Activity: IC_{50} (nM)

Compound	Structure	ERK2	MEK1	MEKK1
1 f152A1	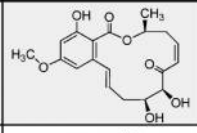	107	<10 (6nM:Astellas publications)	168
2 ER-803064	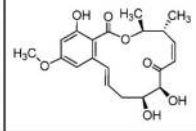	>1,000	82	163
3 E6201	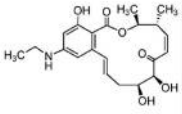	>10,000	5.2	31

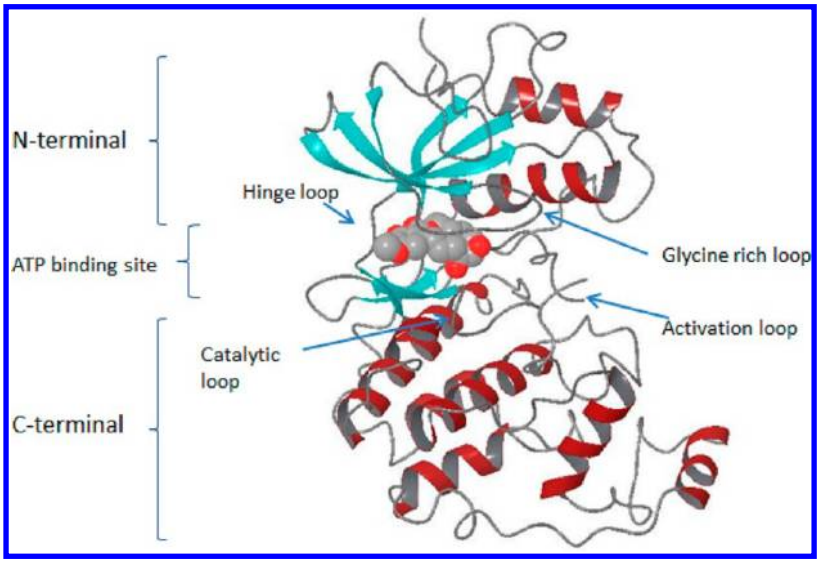

Figure 2. X-ray crystal structure of ATP bound to cAMP-dependent protein kinase (PDB code 1ATP).

activity against ERK2 (IC50 value > 1000; Table 1) while it showed activity against MEK1 and MEKK1 comparable to f152A1.

The changes in kinase enzymatic activities through structure modifications intrigue us to investigate the catalytic binding sites and their fit with these inhibitors. Due to limitation of available X-ray crystal structure analysis on these kinases, we conducted our initial studies in silico.

The protein kinase is organized in a two-lobe structure, whereby the N-lobe, comprised of five twisted β-sheets and a single α-helix, is connected to the mostly α-helical C-lobe by a hinge region. The N-lobe and hinge regions are mainly responsible for nucleotide such as ATP binding and provide part of the catalytic residues, whereas the C-lobe is responsible for substrate binding and catalysis (Figure 2).

Most of inhibitor binding takes place in the ATP binding site, a deep cleft between the N- and C-lobe. Important structural motifs are the glycine-rich nucleotide binding loop, the activation loop, and the catalytic loop. The activation loop is an essential element for the regulation of kinase activity. The activation loop begins with a conserved Asp−Phe−Gly (DFG) motif and ends with a Pro that is conserved among tyrosine kinases. Auto phosphorylation of tyrosines present in the activation loop has been shown to be essential for stimulation

dx.doi.org/10.1021/ci300135g | J. Chem. Inf. Model. 2012, 52, 2059−2068

of activity. In the absence of phosphorylation, the activation loop is not properly positioned for catalysis and prevents binding of ATP and/or substrate. Phosphorylation events in the activation loop cause a significant structural change and stabilize a conformation in which the active site is accessible to substrates, and residues important for catalysis are positioned properly (Figure 3).

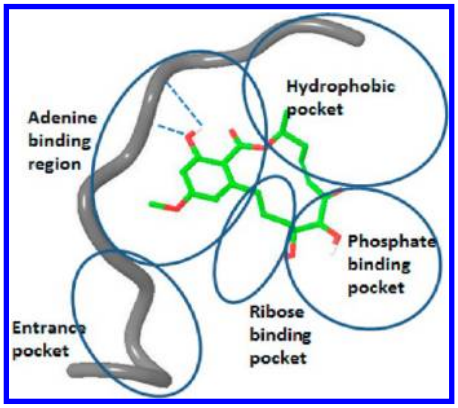

Figure 3. Schematic of ATP binding site and its five pockets. f152A1 is presented in green color, and kinase five pockets at the ATP binding site are marked by a circle line.

Traxlera et al. pointed out that the ATP binding site is made up of five pockets lined by 36 residues being in van der Waals contact and/or involved in hydrogen bonds with the inhibitor.[13]

The presence of a cysteine residue in the active site of each of ERK2 and MEK1 is consistent with the postulated Michael addition reaction and our finding that higher reactivity of the *cis*-enone, among other features, correlates with higher potency of inhibition in vitro. However, f152A1 can also inhibit MEKK1 kinase activity where there is absence of the corresponding cysteine residue at the active site. This led us to carry out additional studies of f152A1 and its analogs to understand the mechanism of MEKK1 inhibition. To answer the question, it is useful to compare the binding modes of f152A1 and ER-803064 with ERK2, MEK1, and MEKK1. In this paper, we describe (1) the conformational analysis of ER-803064 and E6201, (2) modeling of MEK1 and MEKK1 structures from the crystal structure of ERK2, and (3) docking simulation of f152A1 and ER-803064 with ERK2, MEK1, and MEKK1. The docking simulation revealed that the binding mode of f152A1 to MEKK1 is different from ERK1 and MEK1.

The X-ray crystal study revealed that FR148083 (f152A1) binds to the ATP binding site of ERK2.[7] FR148083 (f152A1) formed a covalent bond with the Sγ of ERK2 Cys166 next to the DFG motif (Figure 4). Formation of a covalent bond in the ERK2/f152A1 complex assures that the inhibitor has high

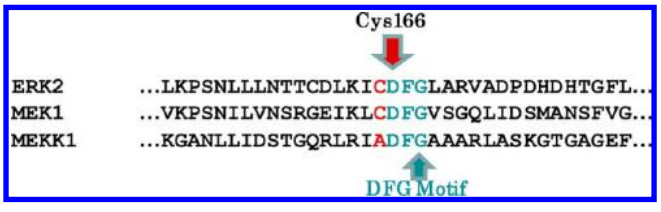

Figure 4. Sequence alignment around the DFG domain in the active site of *human* ERK2, *human* MEK1, and *human* MEKK1.

activity for ERK2. Other kinases of the MAPKK family which contain a cysteine residue corresponding to Cys166 of ERK2 may be similarly susceptible to the covalent modification. If so, covalent binding to the common cysteine residue in the ATP-binding site is likely to play an important role in the inhibitory activity for these MAP kinases. Sequence alignment of human ERK2, human MEK1, and human MEKK1 reveals that MEK1 has a cysteine residue in the ATP binding site corresponding to ERK2 Cys166. On the other hand, MEKK1 has alanine residue which corresponds to ERK2 Cys166. If we postulate that the Michael addition reaction at the *cis*-enone moiety of these compounds as the possible mechanism of inhibition, then it is possible to explain the weak activities of f152A1 (**1**) and ER-803064 (**2**) toward MEKK1; however, it cannot explain the inactivity of ER803064 toward ERK2.

RESULTS AND DISCUSION

1. Conformational Analysis of ER-803064 (2) and E6201 (3). To obtain all possible low-energy conformations of the flexible 14-membered resorcylic acid lactone, we searched the low-energy conformations of ER-803064 (**2**) and E6201 (**3**) by HTMD simulations[13] using the AMBER[14] program as described in the previous report. All snapshot structures in the stored frames were subjected to energy minimization calculation continuously using MMFF (Merck Molecular Force Field[15]). The snapshot structures were subsequently classified into various types of ring conformations according to the set of 14 torsion angles of the 14-membered ring. Structures were classified by every corresponding torsion angle within a tolerance value of 30°. From among these classifications, we selected the 25 lowest energy conformations in the energy range of 10.0 kcal/mol. Then, they were subjected to energy minimization by molecular orbital calculation using MOPAC AM1 PRECISE optimization.[16]

Among low energy conformers of three compounds, M1(8) conformations are the most stable conformation in all three compounds (Table 2). And the M1(8) conformer seems to be an active conformation for all three compounds. Molecular shapes of 2 and 3 are very similar to that of 1 (Figure 5).

Table 2. Heat of Formation Energies and Orbital Energies of Lowest Energy Conformations

compound	conformation	kcal/mol	eigenvalue[a] (eV)	relative reactivity[b]
1 f152A1	**M1(8)**	**−254.12**	**−0.32410**	**0.0**
2 ER-803064	M1(8)	−253.52	−0.32502	−0.00092
3 E6201	M1(8)	−250.67	−0.28097	0.04313

[a](*L* + 1)UMO orbital eigenvalue extending over enone moiety. [b]Relative reactivity for Michael reaction as compared with the enone moiety of 1_M1(8). Eigenvalue difference from enone moiety of 1_M1(8).

2. Protein Structure Preparation. The coordinates for human-ERK2 was obtained from the RCSB Protein Data Bank (PDB entry code: 2E14). Structures were prepared using the Maestro software package. Hydrogen atoms were added, and a brief relaxation was performed on each starting structure using the Protein Preparation module in the Maestro. MEK1 and MEKK1 structure models were built using the Prime homology modeling program. The ERK2 crystal structure (2E14) was used as the template structure (Figure 6).

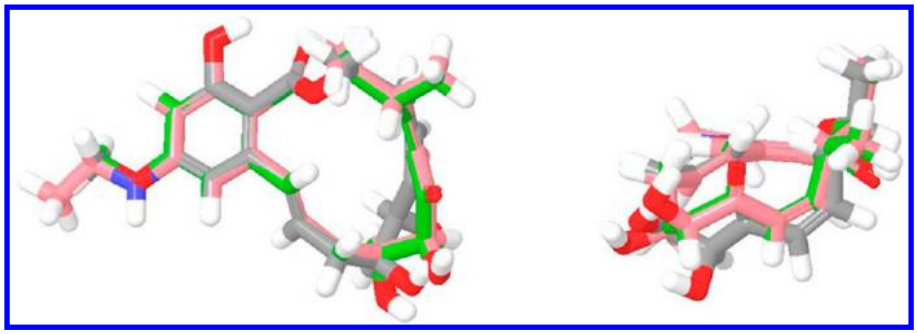

Figure 5. Superimposition of M1(8) conformation of f152A1 (**1**), ER-803064 (**2**), and E6201 (**3**). **1** is presented in gray, **2**, in green, and **3**, in red.

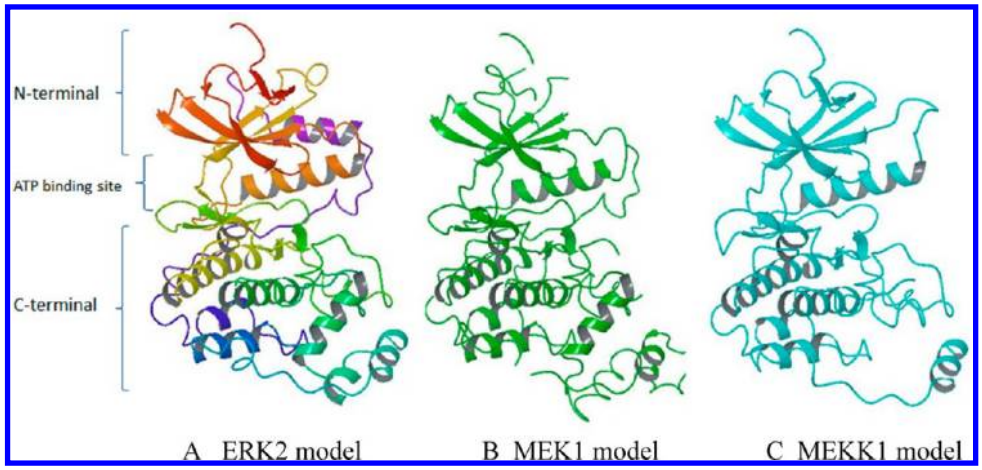

Figure 6. Model structures of ERK2, MEK1, and MEKK1.

3. Induced Fit Docking Simulation with ERK2, MEK1, and MEKK1. We have carried out the induced fit docking (IFD) simulations to predict the ligand binding style by program package Maestro. It is a protein−ligand docking method that accurately accounts for both ligand and receptor flexibility by iteratively combining rigid receptor docking (Glide) with protein structure prediction (Prime) techniques. We have succeeded in reproducing the protein conformational changes like DFG-in/out changes and G-loop conformational changes using this software.

The selected output from the IFD simulations was then subjected to the "QM-Polarized Ligand Docking" simulations as an ab initio methodology to calculate ligand charges within the protein environment using the QM/MM calculations.

1. Induced Fit Docking Simulation of f152A1 with ERK2. Fifteen solutions of docking mode were obtained from the simulation after redocking of f152A1 based on the crystal structure of the ERK2/FR148083 complex.

The top glide score model (rank 1) is selected for further optimization using a QM/MM method. The top five QM/MM Glide scores of the IFD rank 1 model have good scores (Table 3), and each conformation of f152A1 in their models is classified to M1(8) conformation. These models consist of similar binding mode in which the compound binds deep inside the ATP binding site.

The flat aromatic ring fits very well, and the hydroxyl group at C16 forms two hydrogen bonds with main chain atoms of the hinge loop in the adenine binding region. The thickness of the 14-membered ring is located at the ATP binding cleft with several hydrogen bonds to residues at the phosphate and ribose binding pockets. Hydroxyl groups at C8 and C9 make H-bonds with main chain atoms of Ser153 and Lys55, respectively. Also, these hydroxyl groups are located in the solvent-exposed entrance of the ATP binding cleft. The oxygen atom on the C14 forms hydrogen bonding with the main chain amide group at Leu107 and Met108 residues (Figure 7). Main chain and C3-methyl group of the ring occupies the hydrophobic pocket (Figure 7). F152A1 fits well to the wall, but there is no extra space at the complementary place of the C5 atom of f152A1 in the ERK2 active site.

Table 3. Results of QM-Polarized Ligand Docking Simulation of the IFD Rank 1 Model of f152A1 (1) with ERK2

rank	QM/MM glide score
1	−13.576
2	−13.512
3	−13.389
4	−13.380
5	−12.973

C5 atom of f152A1 in the most stable model, M1(8) conformation, and S-atom of Cys166 are in close distance as 3.27 Å. This is a possible distance for the S-atom of Cys166 to react with the C5 atom of *cis*-enone moiety and form a covalent bond. The Michael addition reaction likely occurs in X-ray crystallographic experiments as observed for the ERK2 complex with FR148083 and hypothemycin. However, this contradicts the finding of in-house biological experiments where f152A1 was shown to be a reversible inhibitor of ERK2.

2. Induced Fit Docking Simulation of f152A1 Conformers with ERK2. A good fit was not obtained from the simulation after redocking of the trans form and M1(9) conformer to

dx.doi.org/10.1021/ci300135g | J. Chem. Inf. Model. 2012, 52, 2059−2068

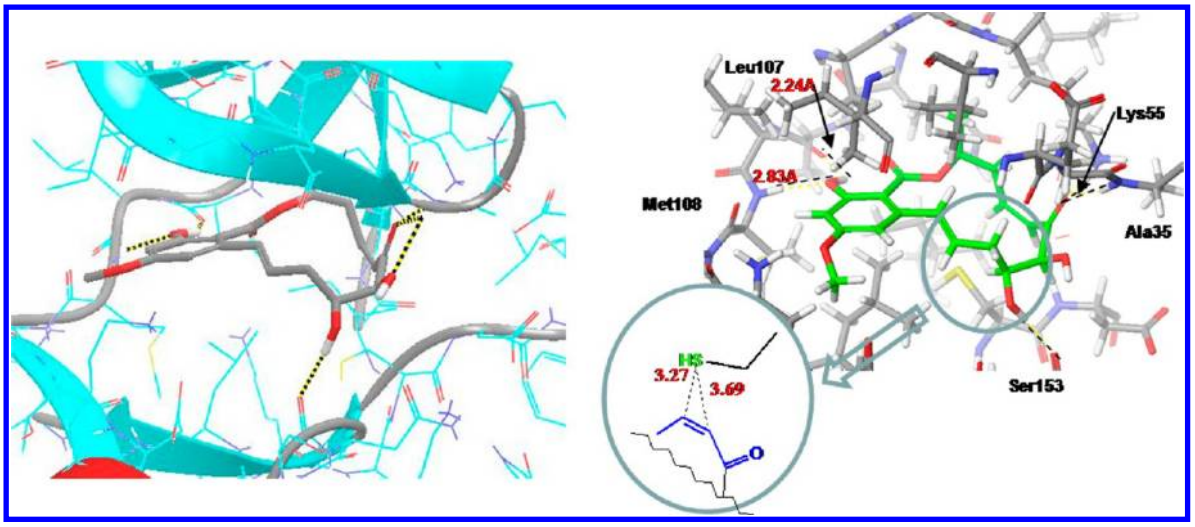

Figure 7. QM/MM rank 1 docking model and binding scheme of f152A1 (**1**) with ERK2.

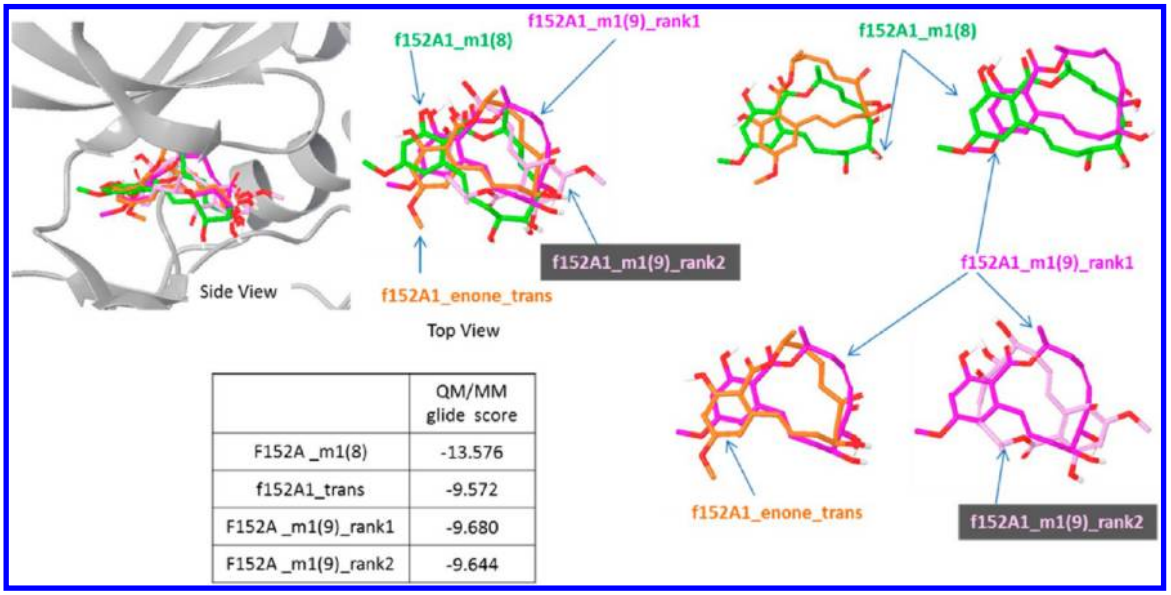

	QM/MM glide score
F152A _m1(8)	-13.576
f152A1_trans	-9.572
F152A _m1(9)_rank1	-9.680
F152A _m1(9)_rank2	-9.644

Figure 8. Comparison of binding mode of f152A1 (**1**) conformers docked with ERK2 by QM/MM simulation. M1(8) is presented in green color, M1(9) rank 1 in purple, M1(9) rank 2 in light purple, and *trans*-enone in orange.

ERK2 crystal structure. Glide scores of the trans form and M1(9) are nearly four points lower than that of the M1(8) conformer (Figure 8).

3. Induced Fit Docking Simulation of f152A1 (1) with MEK1. Some energy stable solutions of docking mode were obtained from the induced fit docking simulation with MEK1 homology model based on the crystal structure of ERK2 (Table 4). The rank 1 docking model is presented in Figure 9a. In this simulation, the rank 1, 2, and 3 models are docked in mostly the same manner; however, in rank 4, interestingly, the compound is horizontally flipped and the methoxy group at C14 is located deep inside the hydrophobic pocket.

Table 4. Results of QM-Polarized Ligand Docking Simulation of f152A1 (1) with MEK1

rank	QM/MM glide score
1	−10.608
2	−10.535
3	−10.349
4	−10.215
5	−10.175

The rank 1 model should be considered as likely f152A1 docking model. The distance between the S-atom of Cys166 and the C5 atom is 3.26 Å, thus the S-atom of Cys166 is accessible to react with the C5 atom at a *cis*-enone moiety and form a covalent bond. The hydroxyl group at the C9 position creates a hydrogen bonding interaction with the oxygen atom of the main chain amide at Ser194. Also, the oxygen atom at the C14 has a hydrogen bond with the backbone of Met148 (Figure 9c).

Interestingly IFD simulation gives two contrasting poses due to the existence of an additional room in the bottom of the hydrophobic pocket. MEK1 has more space in the hydrophobic pocket and wider entrance than ERK2 (Figure 10).

4. Induced Fit Docking Simulation of f152A1 (1) with MEKK1. Seventeen solutions of docking mode were obtained from the simulation after redocking of f152A1 with the homology model of MEKK1 based on the crystal structure of

dx.doi.org/10.1021/ci300135g | J. Chem. Inf. Model. 2012, 52, 2059−2068

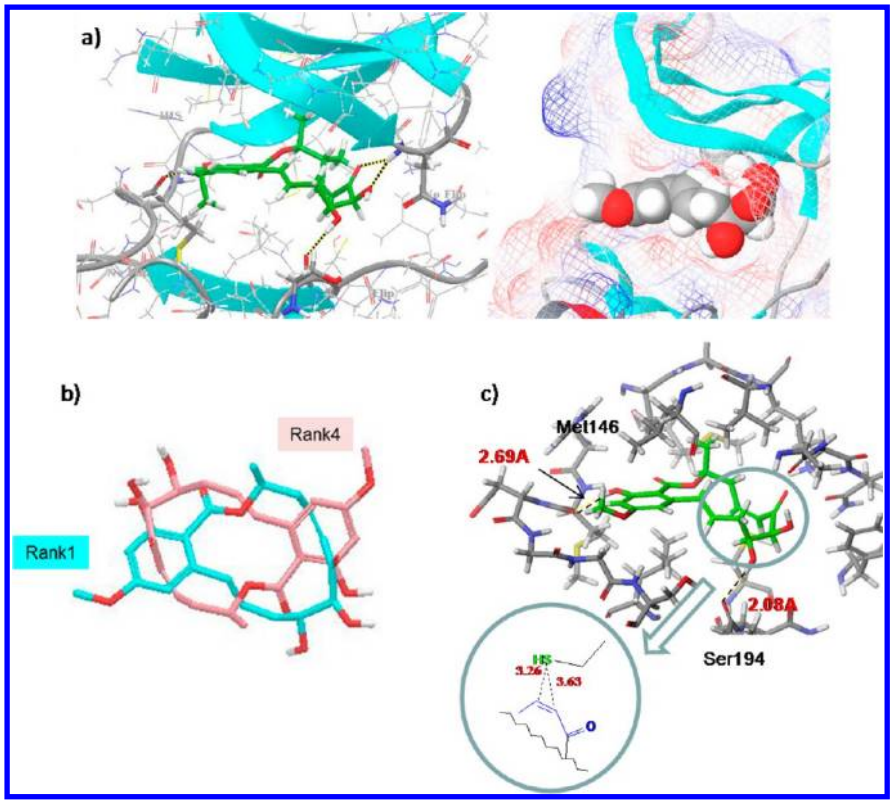

Figure 9. (a) QM/MM-Rank 1 docking model of f152A1 (**1**) with MEK1 presented in (b) superimposition of QM/MM-rank 1 and 4 docking models of f152A1 (**1**) with MEK1; (c) binding site of f152A1 (**1**) with MEK1 complex by QM/MM simulation. Some key residues are also indicated. QM/MM-Rank 1 model is presented in green.

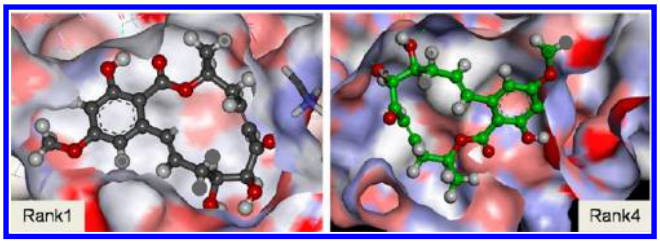

Figure 10. Clipping description of f152A1 rank 1 and 4 in the ATP binding site of MEK1.

ERK2. The top three glide score models were selected for further optimization using QM/MM method. The top five QM/MM Glide scores of IFD model had good value (Table 5).

In this simulation, the rank 3 model is almost same solution with the most stable complex models of f152A1 and ERK2 or MEK1. Rank 1 and 2 are similar models where the compound is horizontally flipped (Figure 11).

Interestingly IFD simulation gives three poses due to the existence of an additional room in the bottom of the hydrophobic pocket. As seen in MEK1 model, MEKK1 model has also more space in the hydrophobic pocket and wider entrance than ERK2.

Table 5. Results of QM-Polarized Ligand Docking Simulation of f152A1 (1) with MEKK1

	QM/MM Glide Score		
rank	IFD rank 1	IFD rank 2	IFD rank 3
1	−10.766	−12.481	−10.696
2	−10.751	−12.294	−10.667
3	−10.570	−12.223	−10.660
4	−10.561	−12.164	−10.493
5	−10.542	−12.095	−10.227

*5. Induced Fit Docking Simulation of ER-803064 (**2**) with ERK2, MEK1, and MEKK1.* Six solutions were obtained from the simulation after redocking of ER-803064 to ERK2 crystal structure. These are classified into two docking modes, and then, the two stable models from each class were subjected to the QM/MM calculation. The IFD rank 2 model produced a 3 points more stable QM/MM model than the IFD rank 1 model (Table 6, Figure 12a).

Eight solutions of docking mode were obtained from the simulation after redocking with MEK1. The first IFD calculation of ER-803064 converged to a stable model for MEK1. The top glide score model (rank 1) is selected for further optimization using the QM/MM method. The top five QM/MM Glide scores of the IFD rank 1 model had good score. All high score solutions have similar binding modes where the compounds are located deep inside the ATP binding site (Figure 12b).

Six solutions of docking mode were obtained from the simulation after redocking with MEKK1. The first IFD calculation of ER-803064 gave three different modes for MEKK1. The top two glide score model (rank 1 and 2) are selected for further optimization using the QM/MM method. Five and ten solutions are obtained from QM/MM Glide simulation of IFD rank 1 and 2, respectively. The highest score solution is obtained from rank 2, and it is similar to the binding mode of f152A1 (Figure 12c).

4. Binding Mode and Kinase Selectivity. As shown in the docking studies, binding of f152A1 and its analogues takes place at the ATP binding site, a deep cleft between the N- and

dx.doi.org/10.1021/ci300135g | J. Chem. Inf. Model. 2012, 52, 2059−2068

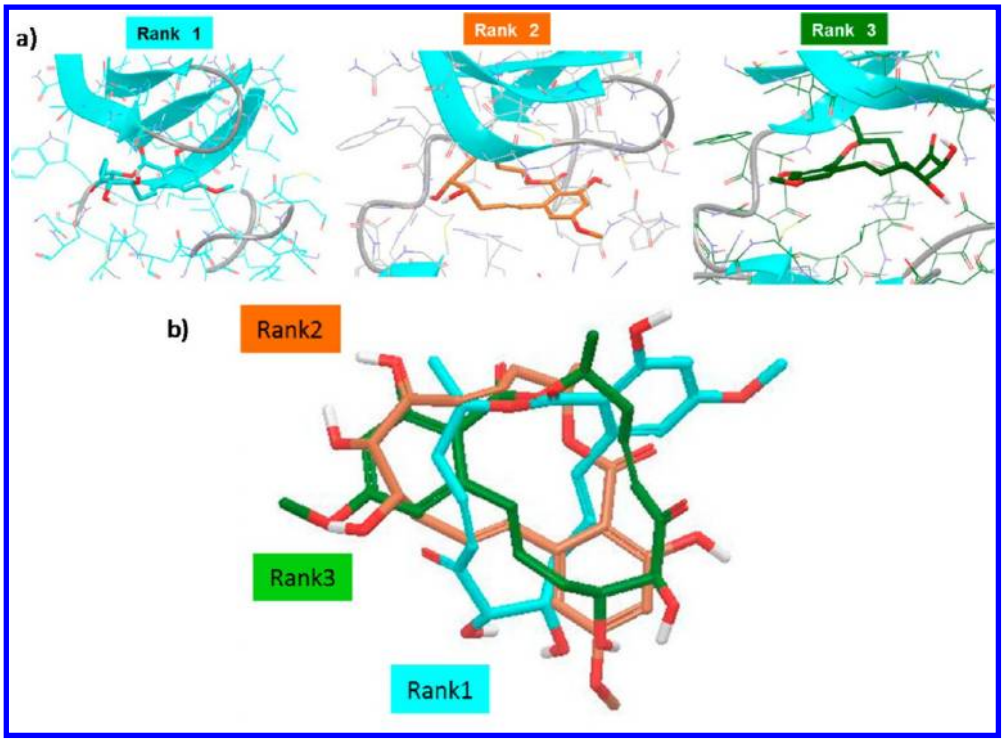

Figure 11. (a) QM/MM-Rank 1, 2, and 3 docking models of f152A1 (**1**) with MEKK1 are presented in (b) superimposition of QM/MM-rank 1, 2, and 3 docking models of f152A1 (**1**) in the ATP binding site of MEKK1 are shown. The rank 1 model is presented in blue, rank 2 is in orange, and rank 3 in green.

Table 6. Results of QM-Polarized Ligand Docking Simulation of ER-803064 (2) IFD Rank 1 and 2 Models with ERK2

	QM/MM glide score	
rank	IFD rank 1	IFD rank 2
1	−8.294	−11.690
2	−8.201	−10.695
3	−8.128	−10.446
4	−8.082	−10.360
5	−8.026	−10.329

C-lobe similar to most kinase inhibitors. Important structural motifs are the glycine-rich nucleotide binding loop, the activation loop, and the catalytic loop. The ATP binding site is made up of five pockets: the entrance pocket, adenine binding region, ribose binding pocket, phosphate binding pocket, and hydrophobic pocket. These pockets are in van der Waals contact and/or involved in the formation of hydrogen bonds with inhibitor. Size and features of the active site cleft are defined by the amino acid sequence of these motifs.

Only f152A1 gives a good model for ERK2 binding as shown in the Table 7. With regards to MEK1 and MEKK1 binding, both compounds gave good binding models.

f152A1 binds deeply inside of the ATP binding site of ERK2 with appropriate hydrogen bonds. ER-803064 is pushed out a little from the cleft and has a shallow contact with hydrophobic pocket (Figure 13).

Both compounds bind deeply inside the ATP binding site of MEK1 with appropriate hydrogen bonds and overlap each other very well at the hydrophobic pocket, ribose pocket, and phosphate binding pocket (Figure 14).

CONCLUSION

We proposed four structural features of f152A1 for kinase inhibition activity in the previous paper.[6] In this study, we discuss the propriety of structural requirement of f152A1 and its analogues using molecular docking techniques. M1(8) conformation is the active conformation because other conformations such as M1(9) and *trans*-enone show less stable binding with ERK2. QM/MM Glide Score shows that f152A1 predicts better binding affinity than ER-803064 by 2 points. This difference can be rationalized by the fact that ER-803064 is located slightly outside of binding pocket as compared to f152A1. So, we conclude that ligand binding affinity correlates with molecular interaction observed in binding models.

We constructed homology models of MEK1 and MEKK1 from the X-ray structure of ERK2. Intermolecular docking studies were carried out for f152A1 and ER-803064 with ERK2 and modeled structures of MEK1 and MEKK1. Every ligands exists in M1(8) conformations at all of the most energy stable complex models. So, these docking simulation studies and conformation analysis results suggest that they bind at the ATP active site in the M1(8) active conformation.

Also, it was suggested where the structural features of f152A1 are well complementary to the interacting amino acids in the active site of these enzymes.

The crystal structure of FR148083 (f152A1) with ERK2 was solved in 2007, and it was found that FR148083 covalently binds to the Cys166 at the ATP-binding site.[7] Docking studies suggested that the interatomic distance between the S atom of Cys166 and C5 carbon of enone moiety of f152A1 is 3.27 Å which is close enough for the Michael addition reaction to occur. It seems that the Michael addition reaction possibly occurs in a certain biological experimental condition, but it

dx.doi.org/10.1021/ci300135g | J. Chem. Inf. Model. 2012, 52, 2059−2068

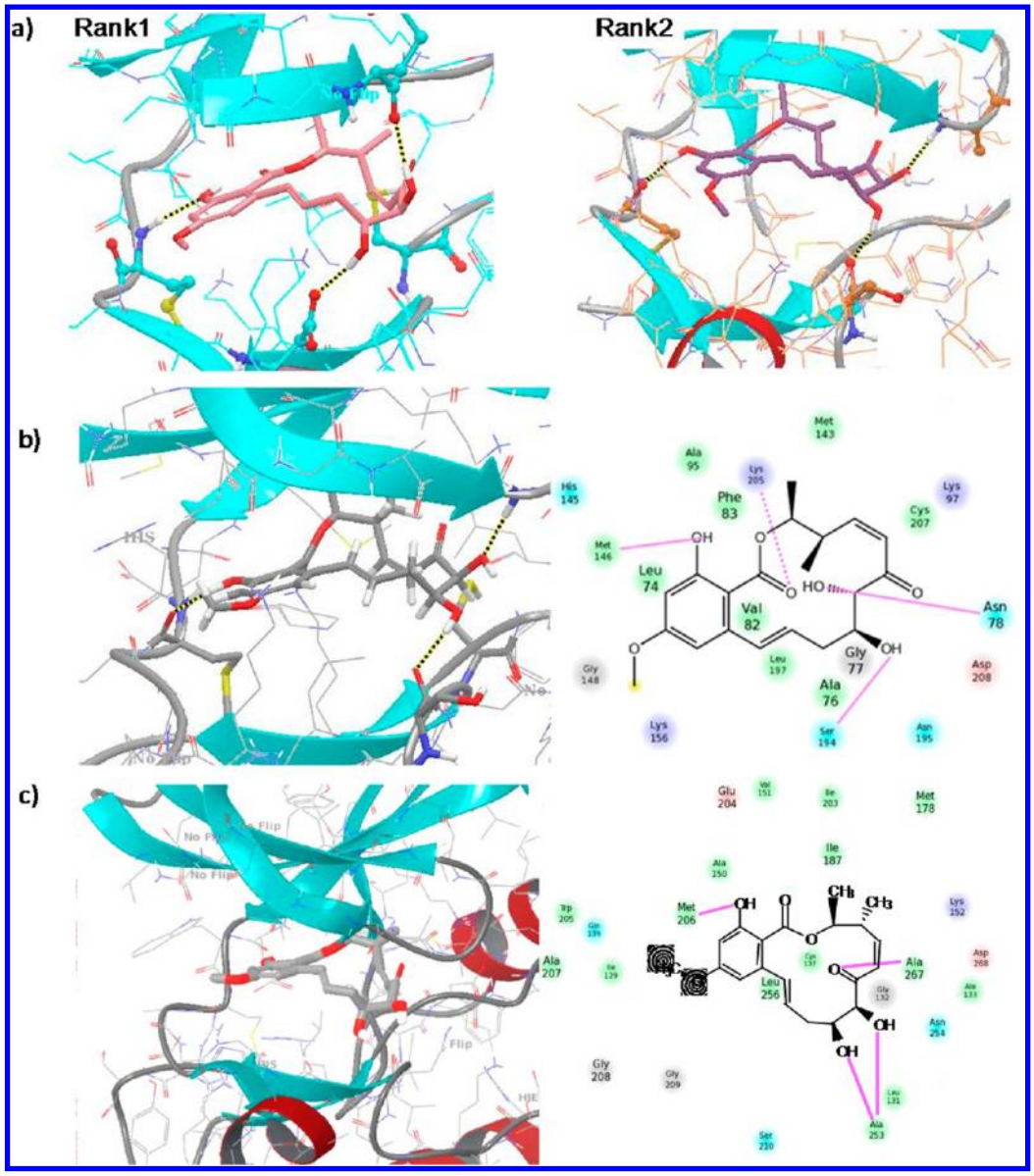

Figure 12. (a) QM/MM-Rank 1 and 2 docking models of ER-803064 (**2**) with ERK2. Rank 1 and 2 models are presented in each figure, and inter H-bonds are indicated by the dotted-line. (b) QM/MM-Rank 1 docking model and binding scheme of ER-803064 (**2**) with MEK1. (c) QM/MM-Rank 1 docking model and binding scheme of ER-803064 (**2**) with MEKK1.

Table 7. QM/MM Glide Scores of the Rank 1 Models of f152A1 (1) and ER-803064 (2) for Three Kinases

	f152A1 (1)	ER-803064 (2)
ERK2	−13.576	−11.690
MEK1	−10.608	−11.771
MEKK1	−12.481	−11.034

contradicts the biological results which suggest a reversible inhibition on ERK2 by f152A1.

f152A1 fits well to the cavity, but there is no extra space at the complementary place of the C4 atom of f152A1 in the ERK2 active site. It suggests that the C4-methyl group of ER-803064 collides the wall and therefore decrease the activity. The docking model with ERK2 suggests that ER-803064 is pushed out from the wall.

We modeled active form of kinases in this study, and we found the f152A1 analogues, ER-803064 and E6201, bind to the region occupied by the adenine ring of ATP (adenine region). They are classified as type 1 inhibitors.[17] Considering their binding mode, it is not always necessary that the DFG motif of the activation loop in the "DFG-in" conformation (kinase active form) for binding. But in these IFD simulations, we have obtained the energy stable complex models in both conformations, DFG-in and -out.

E6201 seems to inhibit both active form and inactive form of ERK2, MEK1, and MEKK1, so additional studies are indicated to further elucidate the SAR of f152A1 and its analogues.

EXPERIMENTAL SECTION

Phosphorylation of ERK2 by MEK1. MEK1 kinase was mixed with ERK2 in assay dilution buffer (ADB) in the presence or absence of compounds. The reaction mixtures were incubated with [γ-^{32}P] ATP for 30 min at 30 °C. Then the reaction was stopped by the addition of SDS-sample buffer. Then, each sample was applied to an 11−14% polyacrylamide

dx.doi.org/10.1021/ci300135g | J. Chem. Inf. Model. 2012, 52, 2059−2068

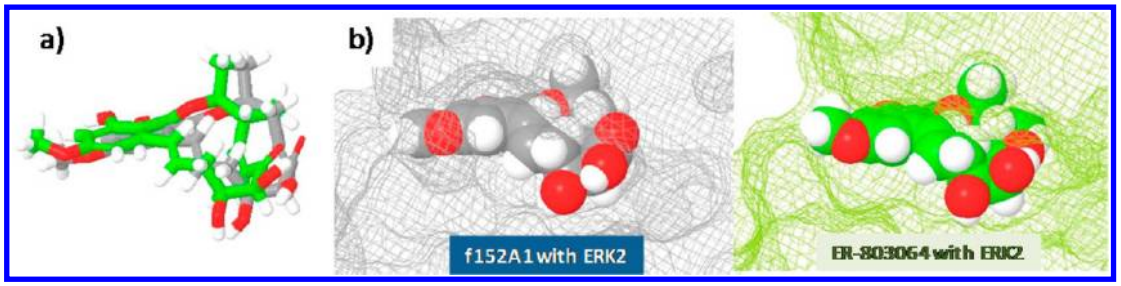

Figure 13. Superimposition and comparison of f152A1 and ER-803064 in ERK2. (a) Superimposition of f152A1 and ER-803064 in the ATP binding site of ERK2. They are presented as stick models, and the carbon atoms of f152A1 are presented in gray. ER-803064 is green. (b) Comparison of f152A1 and ER-803064 in the ATP binding site of ERK2. The solvent accessible surface of ERK2 is presented in the wire model. f152A1 and ER-803064 is presented in the CPK model. ER-803064 is pushed out little bit from the ERK2 binding cleft.

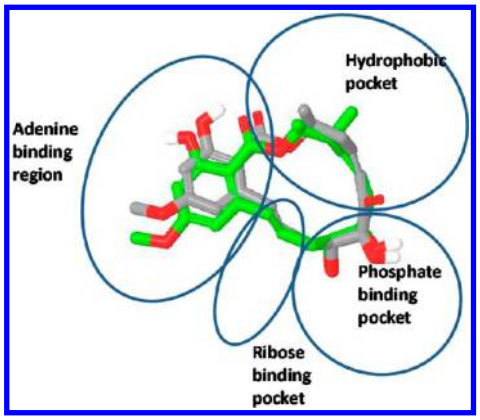

Figure 14. Superimposition of f152A1 and ER-803064 in the ATP binding site of MEK1. Carbon atoms of f152A1 are presented in gray, and ER-803064 is in green.

SDS mini-gel and electrophoresed. The gel was vacuum-dried, exposed to an imaging plate, and the phosphorylated-substrates were analyzed with the BAS2500 system (Fuji Photo Film Co., Tokyo, Japan).

Phosphorylation of MEK1 by MEKK1. MEKK1 was mixed with unactivated-MEK1 in assay dilution buffer ADB in the presence or absence of compounds. Subsequent steps were as described above.

ERK2 Activity Assay. ERK2 was mixed with myelin basic protein (MBP) in ADB in the presence or absence of compounds. The reaction mixtures were incubated with ATP for 30 min at 37 °C. Then the reaction was stopped by the addition of EDTA. Phosphorylated MBP was detected by an ELISA system using antiphospho-MBP antibody and antimouse IgG (goat)-HRP-linked antibody.

Molecular Dynamics Simulations. All the MD calculations were performed using the AMBER program (version 3.0, revision A). For the energy minimization of the stored snapshot structures from the trajectory, a program in AMBER was modified, so as to perform calculations continuously.

Three-dimensional models were prepared on the basis of the crystal structure of "Radicicol". All hydrogen atoms in the molecules were relocated at the geometrically expected positions. The structures were optimized by the MNDO method in the MOPAC program.

The formal atomic charges used for the MD and subsequent molecular mechanics calculations were obtained from those of the optimized structures.

The starting structures were energy-minimized using the same force field parameters as for the MD calculations. Molecular dynamics calculations were subsequently performed for equilibration at 300 K for 10 ps. The high-temperature MD calculations were carried out at 3000 K. The simulations lasted for 100 ps with the time step of 1.0 fs. Solvent molecules were not included in the calculations. The frame data were stored every 50 steps, giving 2000 frames after a 100 ps simulation.

At the beginning of a classification, the template list of referential conformations contained the first frame structure only. Structures whose difference in every corresponding torsion angle was within a tolerance value of 30° were classified into the same ring conformation. If some of the differences were outside the given tolerance values, the structure was added to the template structure list as a new referential conformation. All snapshot structures in the stored frame were subjected to energy minimization calculation continuously by MMFF (Merck Molecular Force Field). Then, the snapshot structures were classified into the typical ring conformations one by one according to the set of 14 torsion angles of the 14-membered ring.

After the classification, we selected the lowest 20 energy structures in the stored frame and they were subjected to energy minimization by MOPAC AM1 PRECISE optimization.

The program package, Discover Studio ver.2.1,[18] was used in superimposition and molecular modeling.

Protein Structure Preparation by Homology Modeling. The coordinates for human-ERK2 was obtained from the RCSB Protein Data Bank (PDB entry code: 2E14). Structures were prepared using the Maestro software package. Hydrogen atoms were added, and a brief relaxation was performed on each starting structure using the Protein Preparation module. MEK1 and MEKK1 structure model were built by means of the Prime[19,20] homology modeling program using 2E14 coordinates as a template structure.

Induced Fit Docking Simulation with QM-Polarized Ligand Docking. We used Induced Fit Docking (IFD)[21] module in the program package Maestro. IFD uses the Glide[22] docking program to account for the ligand flexibility and the refinement module. Prime algorithm implemented in Glide to account for the flexibility of the receptor. Residues within 10 A of the ligand poses were minimized to form suitable conformations of poses at the binding site. Finally, each ligand is redocked into its corresponding low energy protein structures, and the resulting complexes are ranked according to GlideScore. The IFD score is given in kilocalories per mole. It is computed based on the GlideScore, and a small fraction of the Prime energy. The formula is: IFD Score = GlideScore + 0.05 Prime Energy.

dx.doi.org/10.1021/ci300135g | J. Chem. Inf. Model. 2012, 52, 2059−2068

The QM/MM calculation module[23] was used in the QM-polarized ligand docking. This method uses ab initio methodology to calculate ligand charges within the protein environment.

The program package, Maestro ver.9.0,[24] was used in homology modeling and Induced fit docking simulation.

AUTHOR INFORMATION

Corresponding Author

*Phone: +81-29-8475864. E-mail: y-kawakami@hhc.eisai.co.jp.

Notes

The authors declare no competing financial interest.

ACKNOWLEDGMENTS

We are grateful to Drs. Takatoshi Kawai, Tomohiro Matsushima, Young Shen, Hiroshi Shirota, Fabian Gusovsky, and Mr. Kenichi Chiba for their valuable suggestions. We also thank Drs. Lucian DiPietro, Sandra Gilbert, Jean-Christopher Harmange, Masanori Fujita, and Satoshi Yamamoto for providing chemical and biological information.

REFERENCES

(1) Goto, M.; Chow, J.; Muramoto, K.; Chiba, K.; Yamamoto, S.; Fujita, M.; Obaishi, H.; Tai, K.; Mizui, Y.; Tanaka, I.; Young, D.; Yang, H.; Wang, Y. J.; Shirota, H.; Gusovsky, F. E6201 [(3S,4R,5Z,8S,9S,11E)-14-(Ethylamino)-8, 9,16-trihydroxy-3, 4-dimethyl-3,4,9,10-tetrahydro-1H-2-benzoxacyclotetradecine-1,7(8H)-dione], a Novel Kinase Inhibitor of Mitogen-Activated Protein Kinase/Extracellular Signal-Regulated Kinase Kinase (MEK)-1 and MEK Kinase-1: In Vitro Characterization of Its Anti-Inflammatory and Anti hyper proliferative Activities. *J. Pharmacol. Exp. Ther.* **2009**, *331*, 485−495.

(2) Du, H.; Matsushima, T.; Spyvee, M.; Goto, M.; Shirota, H.; Gusovsky, F.; Chiba, K.; Kotake, M.; Yoneda, N.; Eguchi, Y.; DiPietro, L.; Harmange, J. C.; Gilbert, S.; Li, X. Y.; Davis, H.; Jiang, Y.; Zhang, Z.; Pelletier, R.; Wong, N.; Sakurai, H.; Yang, H.; Ito-Igarashi, H.; Kimura, A.; Kuboi, Y.; Mizui, Y.; Tanaka, I.; Ikemori-Kawada, M.; Kawakami, Y.; Inoue, A.; Kawai, T.; Kishi, Y.; Wang, Y. Discovery of a potent, metabolically stabilized resorcylic lactone as an anti-inflammatory lead. *Bioorg. Med. Chem. Lett.* **2009**, *19*, 6196−6199.

(3) Shen, Y.; Du, H.; Kotake, M.; Matsushima, T.; Goto, M.; Shirota, H.; Gusovsky, F.; Li, X.; Jiang, Y.; Schiller, S.; Spyvee, M.; Davis, H.; Zhang, Z.; Pelletier, R.; Ikemori-Kawada, M.; Kawakami, Y.; Inoue, A.; Wang, Y. Discovery of an in vitro and in vivo potent resorcylic lactone analog of LL-Z1640−2 as anti-inflammatory lead, II. *Bioorg. Med. Chem. Lett.* **2010**, *20*, 3047−3049.

(4) Shen, Y.; Boivin, R.; Yoneda, N.; Du, H.; Schiller, S.; Matsushima, T.; Goto, M.; Shirota, H.; Gusovsky, F.; Lemelin, C.; Jiang, Y.; Zhang, Z.; Pelletier, R.; Ikemori-Kawada, M.; Kawakami, Y.; Inoue, A.; Schnaderbeck, M.; Wang, Y. Discovery of anti-inflammatory clinical candidate E6201, inspired from resorcylic lactone LL-Z1640−2, III. *Bioorg. Med. Chem. Lett.* **2010**, *20*, 3155−3157.

(5) Muramoto, K.; Goto, M.; Inoue, Y.; Ishii, N.; Chiba, K.; Kuboi, Y.; Omae, T.; Wang, Y. J.; Gusovsky, F.; Shirota, H. E6201, a novel kinase inhibitor of mitogen-activated protein kinase/extracellular signal-regulated kinase kinase-1 and mitogen-activated protein kinase/extracellular signal-regulated kinase kinase kinase-1: in vivo effects on cutaneous inflammatory responses by topical administration. *J. Pharmacol. Exp. Ther.* **2010**, *335*, 23−31.

(6) Ikemori-Kawada, M; Kawai, T.; Goto, M.; Wang, Y. J.; Kawakami, Y. Conformational analyses and MO studies of f152A1 and its analogues as potent protein kinase inhibitors. *J. Chem. Inf. Model.* **2009**, *49*, 2650−2659.

(7) Ohori, M.; Kinoshita, T.; Yoshimura, S.; Warizaya, M.; Nakajima, H.; Miyake, H. Role of a cystein residue in the active site of ERK and the MAPKK family. *Biochem. Biophys. Res. Commun.* **2007**, *353*, 633−637.

(8) Agatsuma, T.; Takahashi, A.; Kabuto, C.; Nozoe, S. Revised structure of hypothemycin. *Chem. Pharm. Bull.* **1993**, *41*, 373−375.

(9) Schirmer, A.; Kennedy, J.; Murli, S.; Reid, R.; Santi, D. V. Targeted covalent inactivation of protein kinases by resorcylic acid lactone polyketides. *Proc. Natl. Acad. Sci. USA.* **2006**, *103*, 4234−4239.

(10) Nair, M. S. R.; Carey, S. T.; James, J. C. Metabolites of pyrenomycetes. XIV1: Structure and partial stereochemistry of the antibiotic macrolides hypothemycin and dihydrohypothemycin. *Tetrahedron* **1981**, *37*, 2445−2449.

(11) Rastelli, G.; Rosenfeld, R.; Reid, R.; Santi, D. V. Molecular modeling and crystal structure of ERK2-hypothemycin complexes. *J. Struct. Biol.* **2008**, *164*, 18−23.

(12) Kawai, T.; Ichinose, T.; Endo, Y.; Shudo, K.; Itai, A. Active conformation of a tumor promoter, teleocidin. A molecular dynamics study. *J. Med. Chem.* **1992**, *35*, 2248−2253.

(13) Traxlera, P.; Fureta, P. Strategies toward the design of novel and selective protein tyrosine kinase inhibitors. *Pharmacol. Ther.* **1999**, *82*, 195−206.

(14) Weiner, S. J.; Kollman, P. A.; Case, D.; Singh, U. C.; Ghio, C.; Alagona, G.; Profeta, S.; Weiner, P. K. A new force field for molecular mechanical simulation of nucleic acids and proteins. *J. Am. Chem. Soc.* **1984**, *106*, 765−784.

(15) Halgren, T. A. Merck Molecular Force Field. V. Extension of MMFF94 using experimental data, additional computational data and empirical rules. *J. Comput. Chem.* **1996**, *17*, 616−641.

(16) Stewart, J. J. P. MOPAC A Semiempirical Molecular Orbital Program. *J. Computer-Aided Mol. Des.* **1990**, *4*, 1−105.

(17) Zuccotto, F.; Ardini, E.; Casale, E.; Angiolini, A. Through the "Gatekeeper Door": Exploiting the Active Kinase Conformation. *J. Med. Chem.* **2010**, *53*, 2681−2694.

(18) *Discover Studio*, ver.2.1; Accelrys Software Inc., SanDiego, CA.

(19) Jacobson, M. P.; Friesner, R. A.; Xiang., Z.; Honig, B. On the Role of Crystal Packing Forces in Determining Protein Sidechain Conformations. *J. Mol. Biol.* **2002**, *320*, 597−608.

(20) Jacobson, M. P.; Pincus, D. L.; Rapp, C. S.; Day, T. J. F.; Honig, B.; Shaw, D. E.; Friesner, R. A. A Hierarchical Approach to All-Atom Protein Loop Prediction. *Proteins* **2004**, *55*, 351−367.

(21) Sherman, W.; Day, T.; Jacobson, M. P.; Friesner, R. A.; Farid, R. Novel Procedure for Modeling Ligand/Receptor Induced Fit Effects. *J. Med. Chem.* **2006**, *49*, 534−554.

(22) Friesner, R. A.; Banks, J. L.; Murphy, R. B.; Halgren, T. A.; Klicic, J. J.; Mainz, D. T.; Repasky, M. P.; Knoll, E. H.; Shaw, D. E.; Shelley, M.; Perry, J. K.; Francis, P.; Shenkin, P. S. Glide: A New Approach for Rapid, Accurate Docking and Scoring. 1. Method and Assessment of Docking Accuracy. *J. Med. Chem.* **2004**, *47*, 1739−1749.

(23) Cho, A. E.; Guallar, V.; Berne, B.; Friesner, R. A. Importance of Accurate Charges in Molecular Docking: Quantum Mechanical/Molecular Mechanical (QM/MM) Approach. *J. Comput. Chem.* **2005**, *26*, 915−931.

(24) *Maestro*, ver.9.0; Schrödinger, LLC, Portland, OR.